

SLOVAK UNIVERSITY OF TECHNOLOGY IN BRATISLAVA
Faculty of Electrical Engineering and Information

Ing. Marek Búran

Dissertation Thesis Abstract

**Thermal stability of MgB₂ composite superconductors
at high current densities**

**Submitted to obtain the academic title of
„philosophiae doctor“, abbreviated as „PhD.“**

In the doctorate degree study programme:	Physical Engineering
In the field of study:	Electrical and Electronics Engineering
Form of Study:	full-time

Bratislava, November 2023

Dissertation Thesis has been prepared at

Institute of Electrical Engineering, Slovak Academy of Sciences

Submitter: Ing. Marek Búran

Institute of Electrical engineering, Slovak Academy of Sciences
Dúbravská cesta 9, 845 11, Bratislava, Slovakia

Supervisor: Ing. Pavol Kovač, DrSc.

Institute of Physics, Slovak Academy of Sciences
Dúbravská cesta 9, 845 11, Bratislava, Slovakia

Readers: Dr. Elena Fernández Martínez

Instituto de Nanociencia y Materiales de Aragón
(CSIC-Universidad of Zaragoza), Zaragoza, Spain

doc. RNDr. Tomáš Plecenik, PhD.

Univerzita Komenského, Fakulta matematiky, fyziky a informatiky
Bratislava, Slovensko

Dissertation Thesis Abstract was sent

Dissertation Thesis Defence will be held on

at Institute of Electrical engineering, Slovak Academy of Sciences, Dúbravská cesta 9, 845
11, Bratislava

prof. Ing. Vladimír Kutiš, PhD.

Dean of FEI STU

Contents

1	Introduction.....	4
2	Experimental apparatus and measuring system	5
3	Stability of MgB ₂ wires under different cooling conditions	7
4	Thermal stability tested by pulse current measurement.....	11
5	Numerical modelling	15
6	Conclusion	21
7	Bibliography	22

1 Introduction

Functionality of many modern devices, used in research, industry or medical sector is based on magnetic field generation. This requirement is in generally secured by coils which specifications as the wire materials, dimensions, shape or number of turns is adapted to value and shape of generated field. Meet the requirement of high field generation, the fabrication of normal copper coils start to be unprofitable and even impossible to make. In that case a normal conducting wire is exchanged by superconductor. For applications and devices which operate in medium range of fields up to 5T is MgB₂ promising superconducting material. Its price and fabrication process are much more convenient. Therefore, MgB₂ is a promising candidate for many power applications and devices [1].

Composition of practical MgB₂ conductors consist of superconducting filaments embedded in a metallic matrix, frequently noticed as sheath. Metallic sheaths influence not only the conductor processing at room temperature, but also have effect on basic properties at low temperature e.g. transport critical currents properties, current transfer between filaments and sheaths, thermal stability and tolerance to mechanical strength. Definitely, choice of the sheath material is important for the thermal stability of composite conductor.

Temperature of MgB₂ application is considered in the range from 4.2 K to 30 K. Higher temperatures can be obtained by dry cooling with cryocooler and lower ones, e.g. 4.2 K is reached by liquid Helium bath, where the efficiency of cooling is more pronounced. Searching of a transport limit at 4.2 K at various background fields is an important part for wire characterization. Transport current can be limited by local inhomogeneities or cracks, which cause partial drop in critical current value. Therefore, the electrical stabilization is necessary to avoid a wire damage. The conductor stability can be considered mainly from I-V curve above the critical current criterion I_c . I-V curves bear the information about the current redistribution inside the composite and consequently allows to calculate the power dissipation and conducted Ohmic losses. Calculation of heat dissipation helps to understand an overall behaviour of the composite and its direct effect on the thermal stability, e.g. the transition and recovery processes.

The transport measurements were utilized to characterize the samples with different sheath materials or stabilizations under various cooling conditions. From obtained transport measurement, the Quench power density (P_q) as well as Quench current to critical current ratio I_q/I_c were evaluated and compared among the samples with variable architecture and cooling conditions of liquid helium and other methods e.g. subcooled water ice or solid Nitrogen ice. The simulation of DC transport measurement was performed for multifilamentary MgB₂ wire under subcooled water ice at self-field, which exhibits a good agreement with measurement. The new method for determination of electrothermal stability was also established by using the multi-pulse current source. The obtained results of this work can be useful for the design of superconducting coils, cables and other low temperature devices.

2 Experimental apparatus and measuring system

Typically, the characterization of MgB_2 superconductors is carried out under standard conditions with liquid helium (LHe) cooling, which maintains a temperature of approximately 4.2 K at atmospheric pressure. The use of liquid coolant, such as LHe, ensures a uniform temperature distribution and facilitates ease of manipulation during experimentation. The sample characterization at temperatures above 4.2 K are more complicated. The liquid Helium could be considered for temperature up to 5.2 K at a higher pressure. Moreover, the lack of He gas, in combination with increasing demands and production difficulties have increased the price of He over the last years. But, there are several solid media, which can be possibly used for safely cooling. The main coolant requirements used for superconducting systems are high thermal capacity and conductivity. It should be also chemically inert, electrically insulating and low cost. Such coolants can be tested in Cryogen free system based on cryocoolers with sufficient cooling power. Therefore, we developed new system aimed for cryogen-free measurement in external magnetic field, see Figure 1.

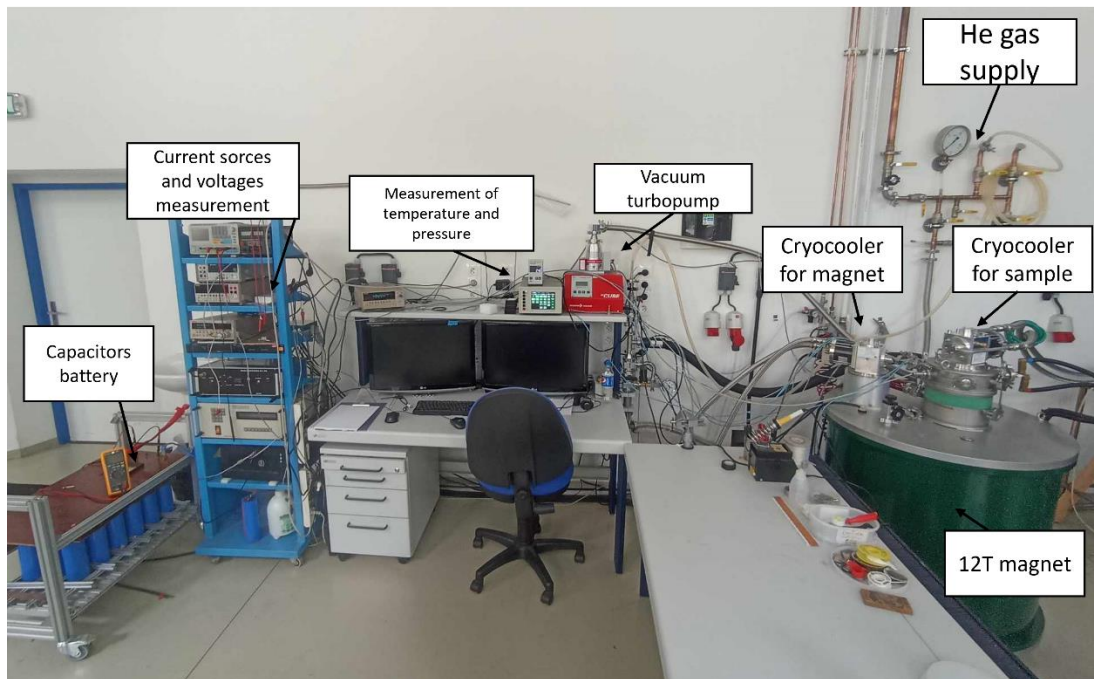


Figure 1 Workplace for cryo-free measurement in external magnetic field

The body of cryostat is made of stainless steel. The main chamber is thermally insulated from ambient room temperature by high-vacuum outer chamber in which a several layers of super-insulation is wound to prevent the sample against the thermal radiation. High vacuum in cryostat outer ($\sim 10^{-6}$ Pa) is provided by Pfeiffer turbopump. The view of cryostat assembly with main parts description is shown in Figure 2 b).

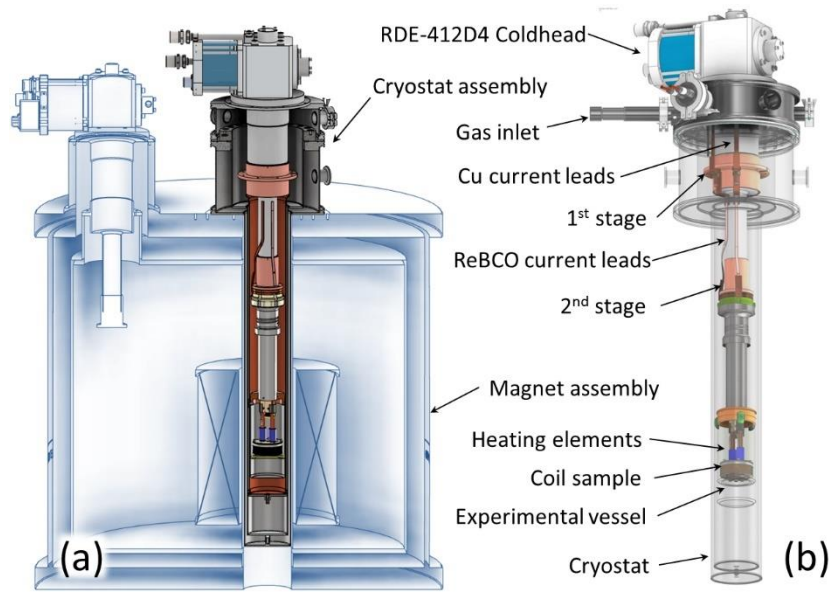


Figure 2 Cryogen-free system for short sample and small coil measurement place in warm hole of 12 T magnet

It is challenging to reach as low temperature as possible during a short time. 30 cm long ReBCO tapes have been used between the 1st and 2nd stage of the cryostat to minimize the heat transfer along the current leads into cryostat interior. In order to achieve a good thermal contact between the cryocooler cold head and the electrically insulated current leads with sample holder, the 50 μm thin Capton foil was not possible to reach the temperature lower than 40 K on the sample. Therefore, a thin (0.3mm) monocrystalline zirconium substrate with excellent thermal conductivity and high electrical resistance at cryogen temperature has been used to separate the cryocooler and cold head which allows to reach the temperature below 25 K. A cooling down test was conducted under low vacuum (>1 Pa at 300K) and under normal pressure of He gas (100 kPa at 300K). The temperature of sample as the function of time in vacuum and He gas is shown by Figure 3 a).

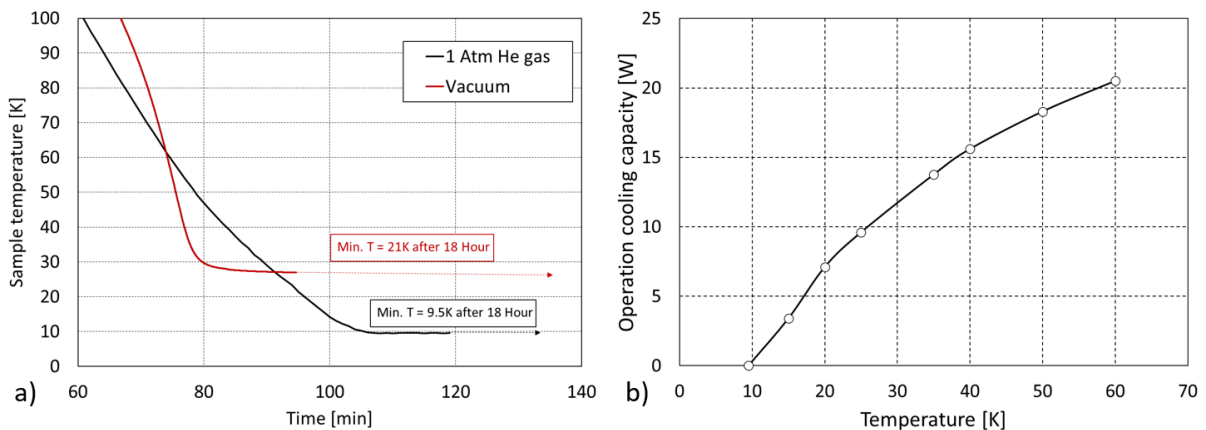


Figure 3 The temperature as the function of time in space of cryostat under different cooling down conditions a), Operation cooling capacity of the measuring system at 10 kPa pressure of GHe b).

As one can see, the temperature around 62 K was reached after ~ 75 min. The temperature 30 K was measured after ~ 80 min in vacuum in comparison to 90 min with He gas. However, the slope of temperature decrease is significantly lower in Vacuum than for He gas slow allowing to minimal temperature down to 10 K. The minimal temperature of the system with vacuum was reached after 18 hour (21 K), in contrast to He gas system setup, where the minimum temperature 10 K was reached after

2 hours. This difference is attributed to He gas improving the heat transfer among the cryocooler head and other warm parts of cryostat. We assume that the temperature of main chamber inner wall was significantly higher than the sample temperature in vacuumed system setup, this wall radiates to the sample and increase the temperature. On the other hand, the wall temperature of system with He gas was effectively cooled to significantly lower temperature and thus do not contribute to heating of inner chamber space. Continual heat load applied to the second stage of cold head is around 8 W what limits the minimum temperature of sample to ~ 9.5 K. There are combined modes of heat transmission: by conduction through the 300 A current leads and wires, radiation from the cryostat walls, and convection heat transferred by He gas. The cooling capacity at temperature range of 10 – 60 K has been determined as a difference of the cold head cooling capacity and sum of the total heat load and power of heaters necessary to reach the given temperature. As the temperature of the measured sample rises, the operation cooling capacity of the system increases above 20 W at 60 K, see Figure 3 b).

3 Stability of MgB_2 wires under different cooling conditions

To estimate the cooling performance of various coolants we tested 6 filaments MgB_2 wire with rectangular cross-section of size $1.09 \times 1.03 \text{ mm}^2$ prepared by Internal Magnesium Diffusion (IMD) method. Each of superconducting filaments is surrounded by Nb barrier (23.6 %), which is sheathed by CuNi30 alloy (42 %), the Cu core (7 %) was added to the central axis of the composite, see Figure 4.

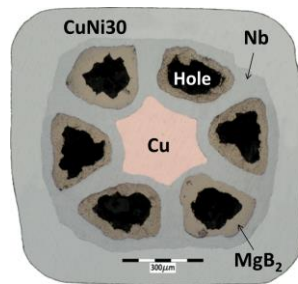


Figure 4 The cross-section of multi-core MgB_2 wire

Firstly, the sample was measured at the temperature range of 34 – 36 K in gaseous helium (GHe) atmosphere maintained at pressure ~ 1 kPa. After that, the GHe was pumped out to reach a vacuum $\sim 0,1$ Pa and the measurement was repeated. The next measurement was performed under condition of SN_2 cooling. The measuring setup was heated up to around 120 K and the plastic container was slowly filled with liquid nitrogen (LN_2). After reaching LN_2 level around 5 cm above the sample and constant temperature of 77 K, the cryocooler was switched on to start the liquid to solid N_2 phase transformation. Pressure in the cryostat chamber gradually decreased during the cooling process due to the effect of trapping the N_2 vapor on cold surfaces. To enhance the cooling process efficiency, a small volume of He gas (200-300 kPa) was added into cryostat chamber at temperature ~ 50 K. The cooling down process for the measurement in water ice was done similarly, like for SN_2 . Just the measuring setup was heated to temperature above 273 K and the plastic container was filled by 0.4 l of deionized water.

Standard DC transport measurement was performed up to the sample quenching under H_2O ice cooling at the temperature range from 33.4 to 36.1K, see Figure 5. $E-I$ characteristics of central part (10 mm) and the whole sample length (50 mm) were measured, Figure 5 a). The comparison of $E-I$ characteristics confirms good homogeneity of MgB_2 wire showing only small current deviations. The $E-I$ differences become more pronounced at higher currents, which can be explained by a heat generation on resistive contacts to current leads and consequent local temperature increase near the sample ends. Figure 5 b) shows the characteristics up to the sample quench in log-dec scale. As one can see, even small change

in the temperature results in relatively large change of I_c , approximately ~ 50 A/K. As can be seen from Figure 5 b), the wire behaves stable at high currents without any sudden thermal runaway at electric fields up to $100 \mu\text{V}/\text{cm}$.

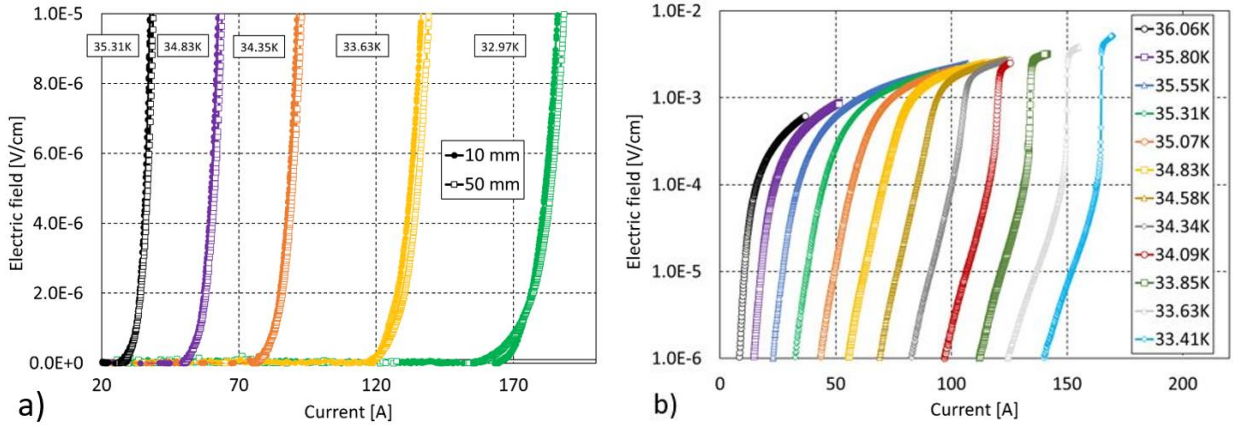


Figure 5 E-I characteristics measured under H_2O cooling condition a) comparison of E-I characteristics measured at 10 mm and 50 mm of MgB_2 wire distance b) E-I measured up to the sample full transition into normal state.

Critical current I_c of the sample measured in H_2O ice and in other cooling conditions was estimated by the criterion of $1 \mu\text{V}/\text{cm}$ and Figure 6 (a) shows the obtained $I_c(T)$ dependences. The temperatures in Figure 6 correspond to the data of Cernox sensor recorded at the moment when the I_c criterion is reached. The step of the temperature during the measurements was systematically decreasing by ~ 0.25 K. As one can see, obtained $I_c(T)$ data follow the same characteristic for each cooling mode, which indicates a correct temperature measurement for given temperature range.

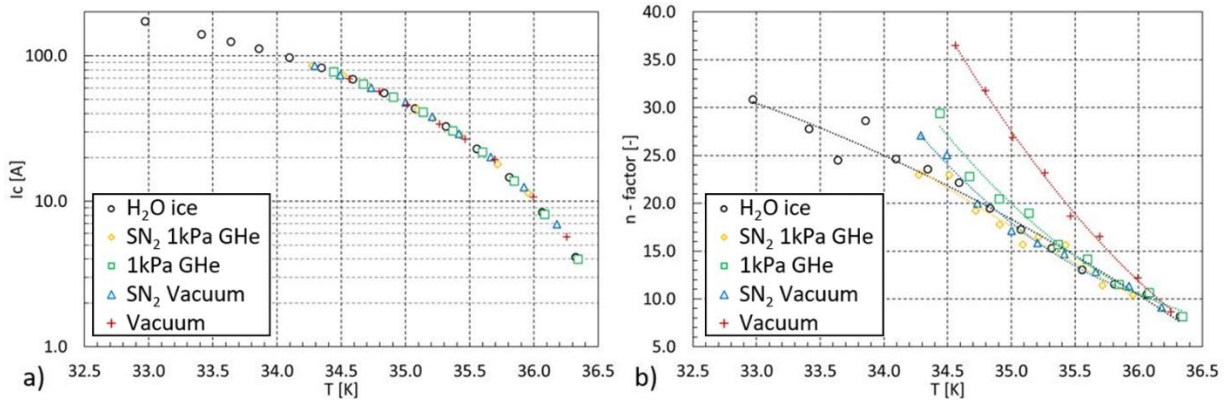


Figure 6 Critical current (a) and n-factor (b) coefficient dependences on temperature evaluated for the temperature range of 33 to 36.4 K

To analyse more the E-I at low electric fields ($1-10 \mu\text{V}/\text{cm}$), n-factor was obtained by fitting of measured data with power-law equation $(E/E_c) \approx (I/I_c)^n$, see Figure 6 (b). Nearly the same n-coefficients are measured for each type of cooling at temperatures above 35 K. But, the n-values higher than for H_2O ice are observed for lower temperatures and also for sample in vacuum at current magnitudes above 10 A. The poorest thermal conditions are observed for vacuum (red crosses), where the sample was cooled only by conduction through the current leads. Little lower n-factors were measured in 1kPa of GHe atmosphere, in which a certain amount of heat is dissipated also by convection. Some difference between the measurements for SN_2 in vacuum and the combination of SN_2 with 1kPa of GHe can be observed. As stated in [2] the nitrogen ice has relatively low dense porous structure and it is difficult to achieve a good thermal contact between SN_2 and sample surface in vacuum. Therefore, adding of gaseous He to the cryostat system results in filling cavities in the nitrogen ice by He molecules and enhances the

cooling efficiency. The best results are observed for measurement in H₂O ice, where the n -factor coefficient increases almost linearly in the contrast to all other measurements where the increase of n indicates an exponential raise.

Figure 7 shows the E - I measured up to quench of sample at temperature ~ 35 K. Due to various cooling conditions, the initial temperatures of the sample were not exactly to the same – it slightly varied around 35 K, which causes small differences of critical currents.

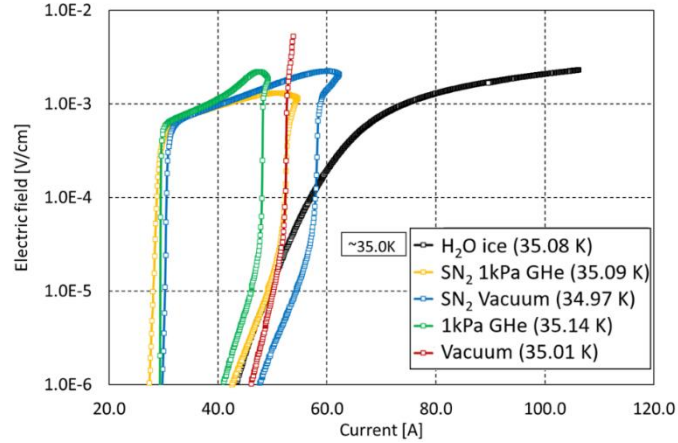


Figure 7 E - I characteristics measured up to quench of MgB₂ sample under various cooling conditions.

From the presented E - I characteristics, the differences in thermal stability among individual cooling methods are clearly visible. According to our expectation, the worst cooling efficiency is observed in vacuum, where immediately after the quench, the temperature increases uncontrollably. On the other side, 1 kPa of GHe still makes a possibility of reversal recovery to superconducting state at transport currents below 50 A. Similarly, for SN₂ in vacuum and GHe, the controlled recovery is possible at transport current up to ~ 60 A, and above this value the temperature increases uncontrollably. The quench of sample was not visible at H₂O ice, because the steepness of voltage does not exceed 100 μ V/A at temperatures above 35 K. Hence, only sample in H₂O ice allows stable operation at critical currents up to ~ 110 A.

Figure 8 (a) shows how the power P depends on the transport current measured under the applied cooling conditions. Due to low thermal response time of the Cernox thermometer (around 200 ms) and slow sampling rate of temperature controller, the temperature change during the rapid transition to normal state could not be recorded. Therefore, no points between the sample quench and normal state are plotted. The sample temperature after transition into normal state was evaluated from measured $R(T)$ characteristics of MgB₂ wire. The sample resistance was calculated as the ratio of V_{tot} and I_{tot} , and each point of the resistance was assigned to the temperature, see Figure 8 (b). Only the temperature for measurements in H₂O ice was measured directly by Cernox sensor, because the ice provided effective thermal stabilization of the sample and transition to normal state was much slower and well controlled.

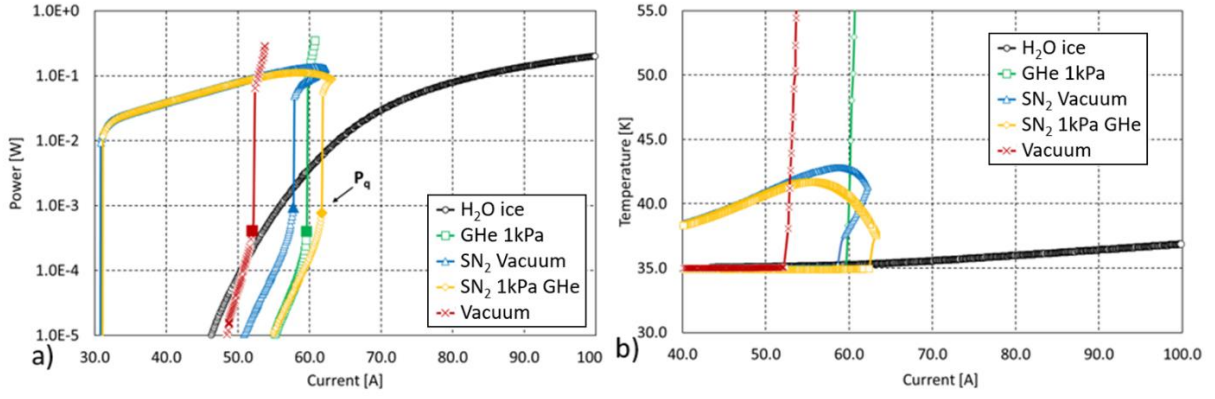


Figure 8 Power (a) and temperature (b) of sample as the function of transport current.

Figure 8 b) demonstrates that the sample temperature changes differently for individual types of cooling. The weakest cooling efficiency was observed for vacuum and GHe atmosphere, at which the temperature after the quench increases rapidly above 55 K. Controllable increase of temperature was observed for SN₂ cooling, however the temperature increases even for decreased transport current. It indicates that the dissipation of the accumulated heat is rather late due to low thermal conductivity of the solid nitrogen. The lowest heating up was observed for measurements in H₂O ice, where $T(I)$ characteristic increases very slightly up to 36.9 K at $I = 100$ A. P_q values are highlighted by filled points at which the quench occurs, see Figure 8 a). The P_q value is defined as the value of the power at which steepness of the voltage raise exceeds 100 $\mu\text{V}/\text{A}$ irreversibly. Figure 9 shows the indicators of transport stability, the quench power P_q depends on quench current I_q in Figure 9 a) and other important parameters reflecting the sample stability, the ratio between I_q and I_c for compared cooling conditions in Figure 9 b).

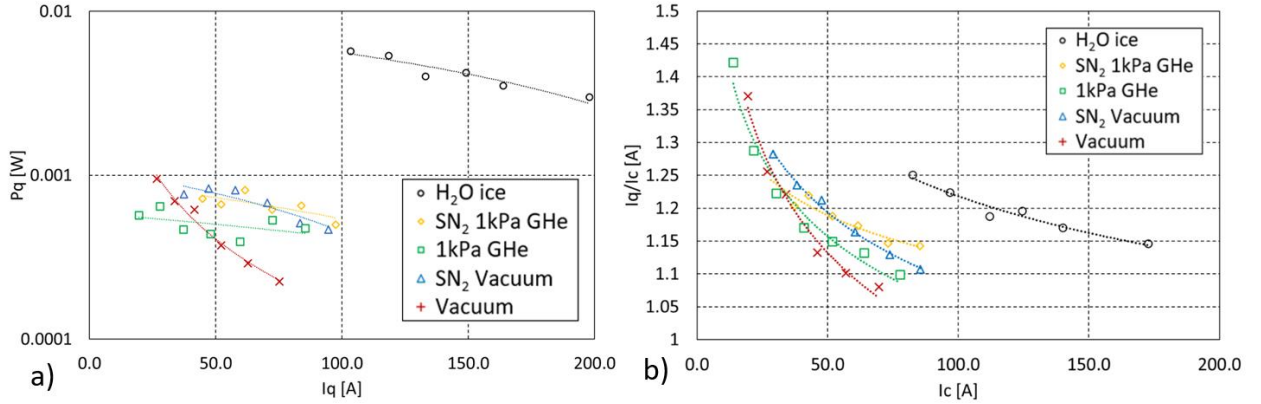


Figure 9 Quench power versus the quench current a) Ratio between I_q and I_c in dependence to I_c for various cooling

To avoid the sample damage, measurements above 100 A were not performed for GHe and SN₂. The measurement in H₂O ice does not show any quench below 100 A. Moreover, the value of P_q in H₂O is more than one order of magnitude higher than for all others at comparable I_q . The lowest P_q is measured in vacuum, which intensively decreases with the current increase. By adding of GHe into vacuum, the sample stability was improved, which is reflected by increased P_q . Cooling with SN₂ allows to increase P_q in comparison to vacuum or 1 kPa helium gas, but not as much as for H₂O ice, which allows to measure at almost doubled transport currents without the sample damage. For $I_q/I_c < 1$ the quench occurs at current lower than I_c value, which can be caused by fluctuation of I_c values along the sample [3]. Figure 9 shows the I_q/I_c ratio versus the critical current. As can be seen, the lowest value of I_q/I_c and its sharpest decrease is observed for the measurement in vacuum. Less gradual decrease of I_q/I_c is observed for GHe and SN₂ combined with vacuum and further improved by the combination of GHe and SN₂. The largest I_q/I_c is evidently measured for the sample in sub-cooled H₂O ice, which clearly demonstrates the best thermal stability of MgB₂ wire.

4 Thermal stability tested by pulse current measurement

The electrothermal stability of MgB₂ composite wire can be tested also by overcurrent pulses. This method has been commonly employed, particularly in the assessment of stability for ReBCO coated conductors (CC), as noted in references [4] [5] [6] [7]. The essence of this method is based on sample ability to withstand the short overcurrent pulse with defined duration without consequent transition to normal state. A key distinction between the convention MQE measurement, which relies on a heat pulse, and the stability measurement based on a current pulse lies in the heat generation process. In the MQE method, heat is applied locally from the external heater, whereas in the current pulse method, the source of heat originates from Joule losses generated within the entire sample volume following the application of an overcurrent. This concept is illustrated in Figure 10, where current pulses include the overcurrent and testing part.

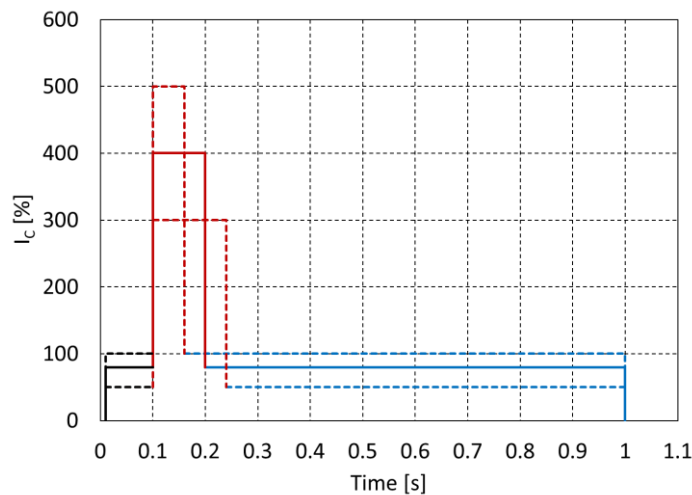


Figure 10 Time dependence of current pulse during electro-thermal stability testing.

The time-dependence of the current pulse can be dissected into these three segments, see Figure 10, and each serves in characterization of sample stability. The initial phase of the pulse (indicated by the black line) serves as an informative starting point, characterized by a current amplitude lower than I_c , usually falling within the range of 50% to 100% of I_c .

The second phase of the pulse (depicted by the red line) guides the sample towards a quasi-stable state, where observable voltage is detected at the voltage tabs. This part of the pulse exhibits a relatively steep incline, with the rate of increase influenced by the self-circuit inductance.

The final segment (denoted by the blue line) corresponds to the evaluation phase, during which the sample either transitions to the normal state if the overcurrent pulse part (OPP) was sufficiently high or stabilizes if it was not. This phase captures the critical moment that determines whether quenching occurs or if the system manages to retain stable.

This measurement involved the utilization of the MP source. This source offers a precise control over the amplitude, duration, and shape of the testing pulse. The stability assessment of W6Cu sample was carried out under self-field and at external magnetic field of 1T. These assessments were conducted using adiabatic and 100 mBar helium gas cooling conditions. The experimental setup involves combined pulses with a total duration of 1100 ms, where the overcurrent component (OPP) spanned 20 ms, followed by an assessment phase of approximately 850 ms see Figure 11.

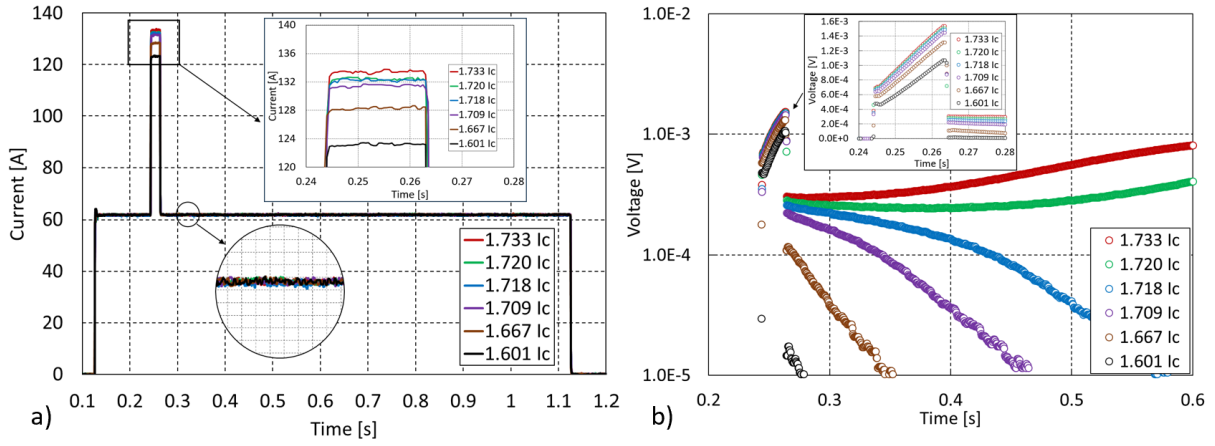


Figure 11 Time dependence of current pulse (a) corresponding Voltage response depends on time under adiabatic conditions at self-field, the offset zoom the detail in dec-dec scale (b).

The time-dependence of current pulse injected into the W6Cu sample led to an increase of voltage along the sample. Voltage measurements were taken at the midpoint with voltage taps positioned 10 mm apart. The applied pulse, shown by Figure 11 a) was adjusted to 80 % of I_c . The amplitudes of the OPP vary from 123 A to 134 A, which is expressed as the multiple of I_c value.

The differences of sample stability become evident by a voltage response shown by Figure 11 b). For tested pulses with amplitudes below $1.718 \times I_c$, included, although the voltage rapidly rises above 1 mV, but during the assessment pulse part, it gradually decreases to zero, indicating a full recovery of the sample. A relatively fast recovery, taking less than 100 ms, was observed following an testing pulse with OPP corresponding to $1.601 \times I_c$. As the amplitude of the overcurrent pulse increases, the time required for recovery is extended, until overcurrent pulses exceed $1.72 \times I_c$, at which the normal zone starts to develop. Furthermore, higher overcurrent amplitudes lead to a faster propagation of the normal zone, eventually culminating in a fully resistive state immediately after the overcurrent pulse part termination. The energy dissipated over the controlled area can be used for assessment of wire ability to resist the irreversible quench. This energy can be calculated by using simple equation:

$$E = (I_{op} - I_c) \int U(t) dt \quad (1)$$

Where the $U(t)$ is the voltage over the sample that varies with time t , I_{op} is the amplitude of overcurrent pulse, I_c is the critical current value. The raise in energy as the function of the time is shown in Figure 12.

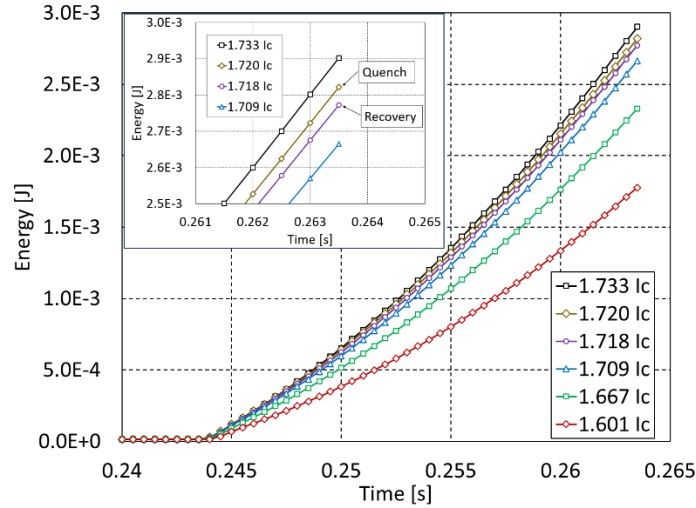


Figure 12 The energy dissipated during the overcurrent pulse part as the function of time, the offsets show the detail with noted the energy limit for recovery/quench development.

The dissipated energy over the recorded part of sample starts to raise at 0.244 ms, coinciding with the activation of the OPP that spans 20 ms. During this interval, the energy growth corresponds to the amplitude of overcurrent pulse. A focus associated with $1.718 \times I_c$ and $1.720 \times I_c$ reveals a threshold value of 2.8 mJ as the critical energy level above which quenching of the sample takes place, see inset of Figure 12.

The stability of the sample at external magnetic field of 1T was investigated by the same method at temperature 30.2 K. The time dependence of pulse current and corresponding voltage response is shown in Figure 13.

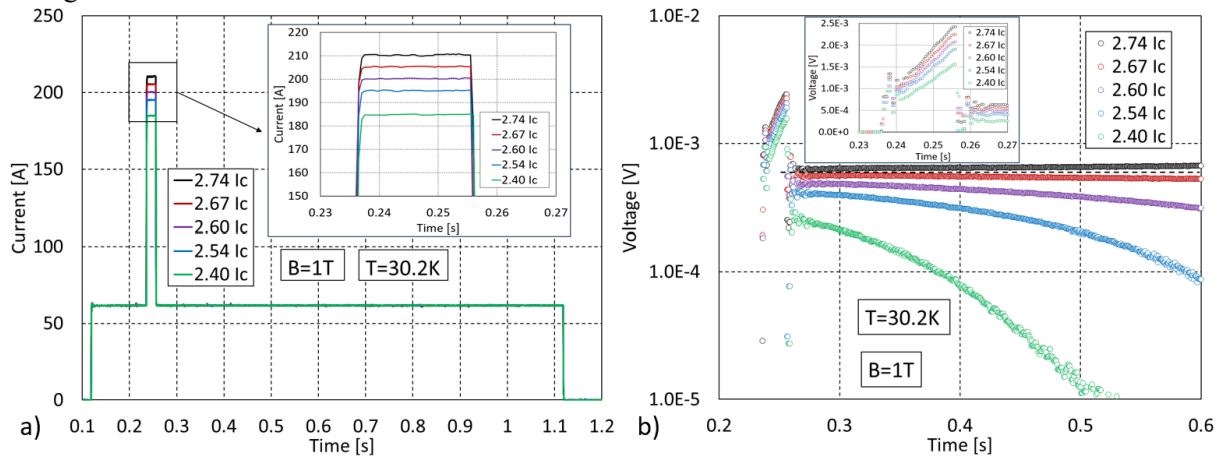


Figure 13 Time dependence of current pulse (a) corresponding Voltage response depends on time under adiabatic cooling conditions at magnetic field of 1 T, the offset zoom the detail in dec-dec scale (b).

Enhanced stability of the sample was observed after application of a 1T magnetic field. The introduction of the magnetic field leads to a reduction in the I_c value. To maintain a consistent I_c value, the temperature was adjusted to approximately 30.2 K, keeping the I_c at 77 A. The influence of the magnetic field is also evident in the V - measurements, with increased noise and distortion observed in the initial part of the V(t) characteristics. A gradual escalation in the magnitude of the overcurrent results in higher voltage along the sample. This evolution continues until a quasi-stable state, after which any further increase in the sample's temperature occurs only upon quenching. In order to induce the quench, an OPP with of $2.74 \times I_c$ was applied into the sample. This value is approximately 1.6 times higher than value applied under self-field conditions. Interestingly, the transition to the normal state is less rapid despite the

considerably higher OPP was applied. Higher OPP induces higher amount of dissipated energy, which is illustrated in Figure 14.

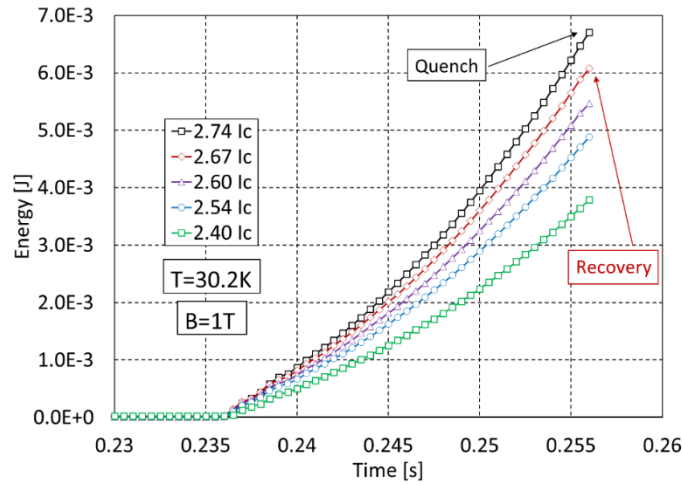


Figure 14 The energy dissipated during the overcurrent pulse part action as the function of time with noted the energy limit for recovery/quench development.

The OPP with an amplitude of $2.67 \times I_c$ induces a dissipation of energy slightly above 6 mJ, which maintains the sample stable, offering the potential for subsequent recovery. However, the pulse featuring an OPP of $2.74 \times I_c$ results in an energy dissipation of 6.7 mJ. Beyond this energy threshold, the sample's stable operation is compromised, leading to an increase in the sample's temperature and preventing recovery.

The results of the stability of W6Cu under variable cooling conditions at self-field and 1T are summarised by Figure 15

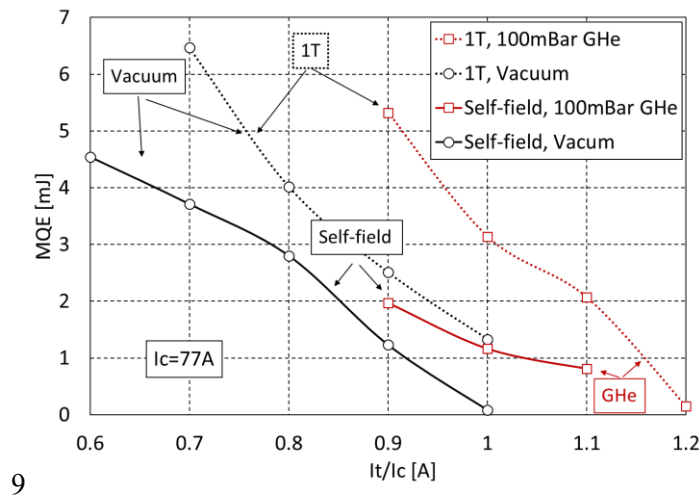


Figure 15 Minimum quench of energy as the result of overcurrent pulses depends on I_t/I_c ratio at self-field and 1T, under adiabatic cooling condition and 100mBar of LHe.

The change in cooling conditions (vacuum-He gas) resulted in an average increase of MQE by ~ 1 mJ. A noticeable reduction MQE was observed during measurements in vacuum after increasing of I_t/I_c ratio beyond 0.8. This observation underscores that even a minor disturbance can lead to sample quench when heat transfer is negligible within the vacuum. The introduction of a helium gas environment at 100 mBar yielded an enhancement of wire stability, evident by the upward shift in the characteristics to higher MQE values. The stability improvement in the presence of helium gas allowed the MQE measurement

beyond the I_t/I_c threshold of 0.8. Furthermore, the application of a 1T magnetic field demonstrated a significant improvement in wire stability.

5 Numerical modelling

In this simulation two MgB_2 wires of different composition but identical dimensions, (W6Cu and W6Nb, described above and presented by [8] and [9], see Figure 16) are modelled. The section of the model pertaining to the superconducting domain was constructed based on the research works of Sirois F. and Lacroix Ch. from the Montreal research group, as documented in [10] [11]

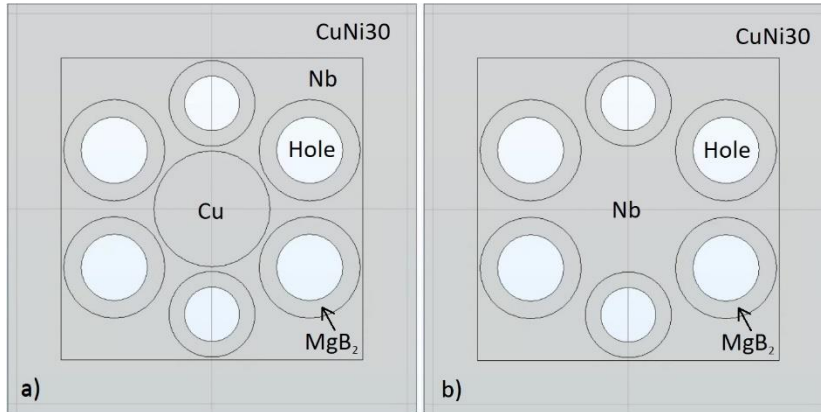


Figure 16 The cross-section of simulated MgB_2 wires a) with Cu core stabilization and b) stabilization free.

The wire model is composed of several distinct domains, each representing individual metal components (CuNi30, Nb, Cu, MgB_2), as well as holes centred within the MgB_2 domain. These holes do not contribute to any electro or thermal effects. The thermal properties of each individual metallic layer were sourced from existing literature [12] [13] and from the COMSOL library. Electrical properties were determined from $R(T)$ measurements. The cross-sectional areas of individual domains were derived from the actual wire composition, which are presented in Table 1.

Table 1 Composition of wires used for simulation and experimental measurements.

	Cross-section (mm ²) (%)	CuNi30 sheath (mm ²) (%)	Nb barrier (mm ²) (%)	MgB_2 (mm ²) (%)	Hole (mm ²) (%)	Cu-core (mm ²) (%)
Experiment MgB_2/Nb	1.1 (100%)	0.5 (45.04%)	0.3357 (30.24%)	0.1404 (12.64%)	0.1239 (11.16%)	x
Experiment MgB_2/Cu	1.11 (100%)	0.51 (45.95%)	0.242 (21.81%)	0.167 (15.05%)	0.121 (10.9%)	0.0698 (6.29%)
Model MgB_2/Nb	1.1 (100%)	0.503 (45.72%)	0.33 (30.1%)	0.146 (12.16%)	0.122 (11.1%)	x
Model MgB_2/Cu	1.1 (100%)	0.503 (45.72%)	0.239 (21.71%)	0.1668 (15%)	0.122 (11.1%)	0.0693 (6.3%)

The subsequent section provides an overview of 3D model developed for two superconducting wires, namely W6Cu and W6Nb, under conditions of standard DC transport measurement discussed in the referenced chapter. Despite of several simplifications, the simulation exhibits remarkable conformity with the experimental results obtained for W6Cu. However, it's important to note that the model for W6Nb demonstrates a weaker agreement, which will be discussed in the subsequent section. The 3D visualization of the W6Nb wire shortly after quench, is shown in Figure 17.

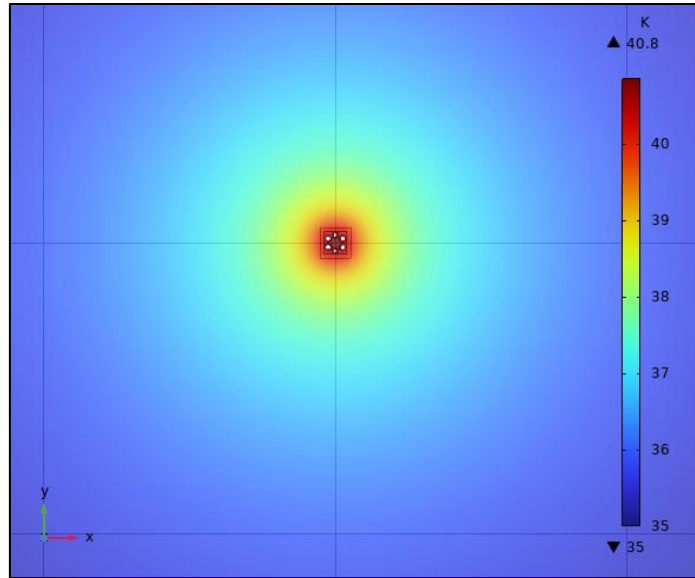


Figure 17 The temperature distribution of W6Nb in water ice domain after the quench.

The initial temperature of the calculation was 35 K and extensive heat distribution in water ice domain was achieved, which indicated well thermal conductivity of the water ice at low temperature. The Figure 18 provide more detailed imagination of longitudinal temperate distribution along the wires before and after quench.

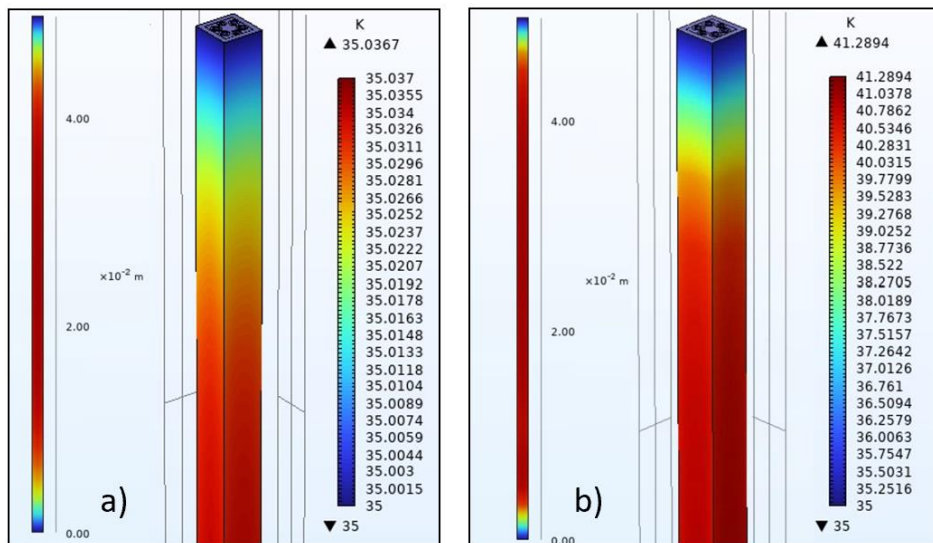


Figure 18 Longitudinal temperature distribution of W6Nb wire under H₂O cooling conditions a) before the quench b) after the quench

Following the quench, substantial temperature gradient becomes apparent along approx. 1 cm length of the sample, as illustrated in Figure 18 b). The extent of thermal distribution is attributed to high thermal conductivity of W6Nb wire. High thermal conductivity results in expansive temperature distribution and reduced temperature gradient, see Figure 18 b). It becomes evident that despite a temperature difference exceeding 6 K, almost entire temperature gradient is distributed to the less than 1 cm at the sample's end. A notably different temperature distribution is shown by Figure 19.

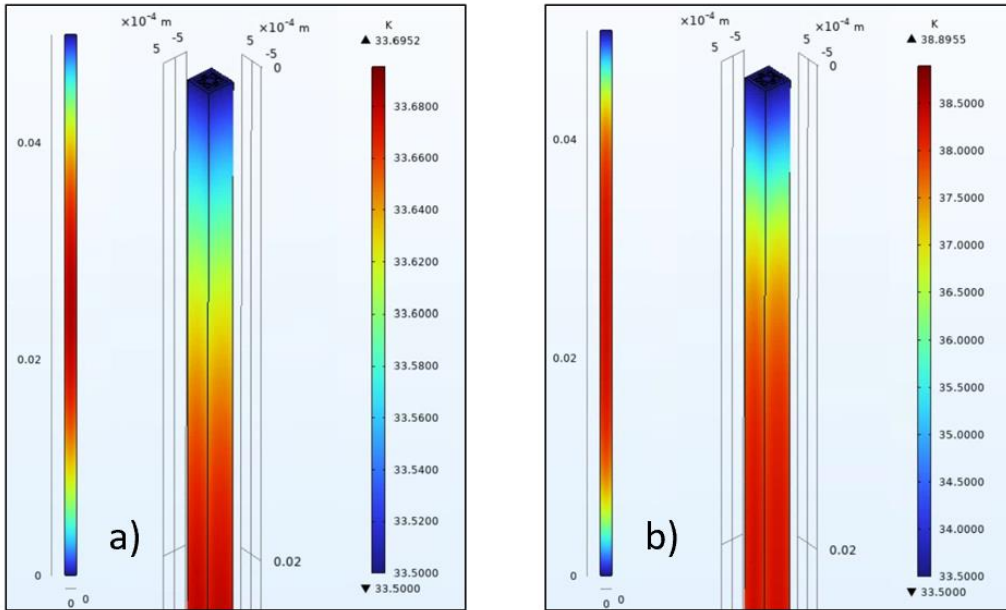


Figure 19 Longitudinal temperature distribution of W6Cu wire under H_2O cooling conditions a) before the quench b) after the quench.

The temperature distribution in W6Cu exhibits a more widespread span, extending to roughly twice the length observed in W6Nb. This reduced temperature gradient in W6Cu is attributed to its higher longitudinal thermal conductivity. Despite W6Cu's thermal conductivity, a relatively modest temperature gradient is evident along a 10 mm segment situated in the middle of sample. For a more comprehensive representation of the temperature profile, the average temperature value along the length of the sample was computed and analysed. This allows clearer mapping of the temperature distribution and offers insights into thermal behaviour of wire before and after quench.

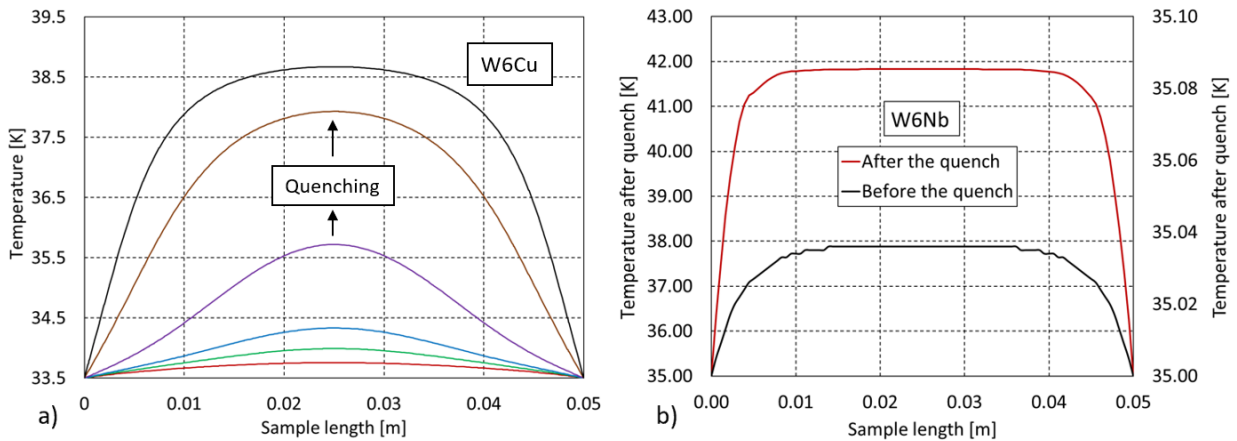


Figure 20 The temperature distribution along the sample a) W6C b) W6Nb

Figure 20 presents the distribution of temperature along the sample before and after quench. In the case of W6Cu, a gradual and relatively slow quenching is evident. The time spanning among each line in Figure 20 a) is shifted by 50 ms. W6Nb exhibits a steep transition into the normal state during less than 50 ms, primarily due to higher power dissipation caused by a higher sample resistance. Despite the notable discrepancies in thermal conductivity between these samples, the temperature distribution along the middle section appears relatively uniform. This uniformity provides an opportunity to simplify the model by focusing on the 10 mm central portion for further analysis. Furthermore, the temperature distribution across the wire cross-section is found to be non-uniform. Figure 21 illustrates this non-

uniformity, which is attributed to variable current density within the individual components of wire. The temperature profiles in the cross-sections provides insights into the heat distribution and dissipation mechanisms within the wire.

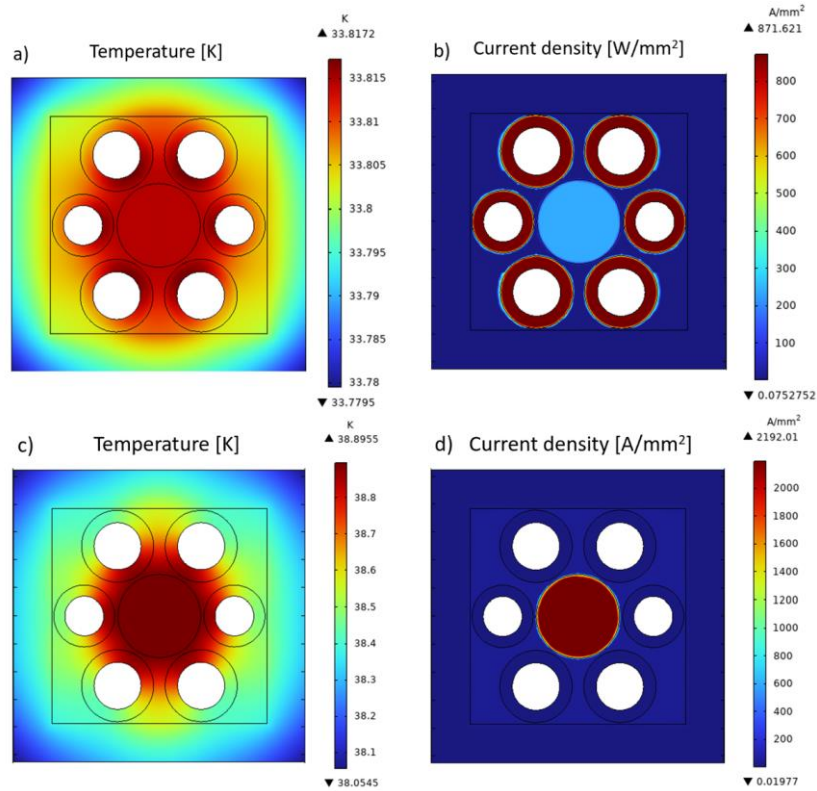


Figure 21 The temperature and current density distribution in W6Cu wire cross-section a), c) before the quench b), d) after the quench

Figure 21 a), c) display the temperature distribution inside the cross-section of compared wires. The highest temperature is observed in the centre of wire and the effect of transverse cooling by water ice is evident in the temperature gradient observed across the wire's diameter. The difference between the minimum and maximum temperatures (ΔT) across the wire's cross-section is relatively small (≤ 40 mK) before quench, but it becomes more pronounced after the quench, resulting in $\Delta T = 0.8$ K. Figure 21 b), d) provides the current density distribution before and after the quench, respectively. At this stage, the entire current density is concentrated within the superconducting filament. However, as the quench occurs, the portion of current begins to flow through the metallic elements of wire. The distribution of the current follows the principle of minimizing electric field (E), leading to the highest current density concentration in the copper core, as depicted in Figure 21 d). This distribution of current density is crucial factor influencing the overall temperature and thermal behavior of the composite wire.

E-I characteristics in Figure 22 show a comparison between numerical model and measured results at the same conditions, (zero magnetic field and the same temperature or current ramping). This comparison aims to examine the fidelity and accuracy of our simulation in with real behavior of superconducting wires cooled by water ice and its ability to capture electro-thermal dynamics of the system.

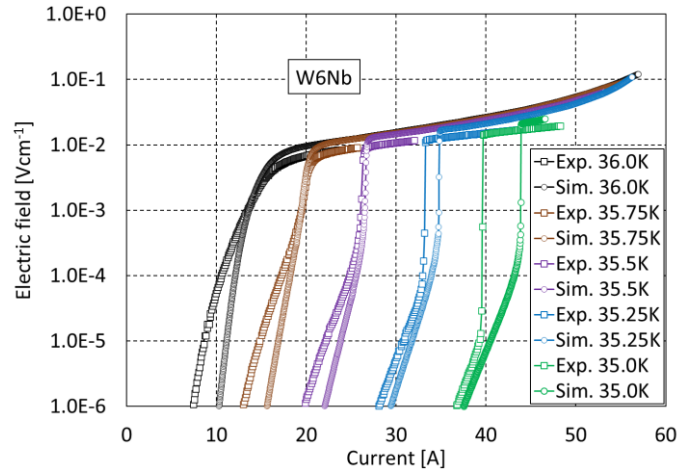


Figure 22 Comparison of E-I characteristics obtained by simulation and measurement at H₂O ice cooling.

Similar electro-thermal behaviour with a smooth transition into normal state is evident at lower currents. As the critical current increases, the transition becomes more abrupt. For critical currents surpassing 20A, a decisive transition to the normal state is clearly observed in modelled and experimental results. Slight differences exist between the two sets of characteristics. Particularly, the discrepancies in critical currents at temperatures proximate to the critical temperature (T_c) are well visible. At these temperatures, the values of critical currents derived from the experiment are significantly lower than I_c obtained by model. However, as temperature rises, a convergence between the characteristics becomes more evident. At temperature $T = 35K$ and corresponding $I_c = 37 A$, the difference in I_c between the experiment and model is less than 1A. Another distinction can be detected in the resistance following the transition to the normal state. The model exhibits a higher electric field in the normal state, caused by elevated resistivity. The higher resistance is closely linked to the higher temperature of the wire in the normal state.

The most visible difference between the model and the measurement lies in the electric field value at quenching. While the experimental data reveals a steep decrease in this value with increasing critical current, the model show relatively stable electric field threshold for quenching. This discrepancy may be explained by local variations of critical current, which could initiate the quenching beyond the controlled zone. This effect is more pronounced for less stabilized samples, where the critical ratio I_q/I_c is lower compared to well-stabilized wires.

The example of better stabilized wire sample is the W6Cu with well conductive cooper. By increasing of current above I_c , the power losses are generated, and the heated sample is close to quench. However, by keeping the same current ramping rate, the losses in well stabilized sample are slower giving a more time for their dissipation. It can be expected that a higher quench power will be in well stabilized sample, compared to poorly stabilized. The comparison of modelled and measured E-I characteristics of W6Cu are shown in Figure 23.

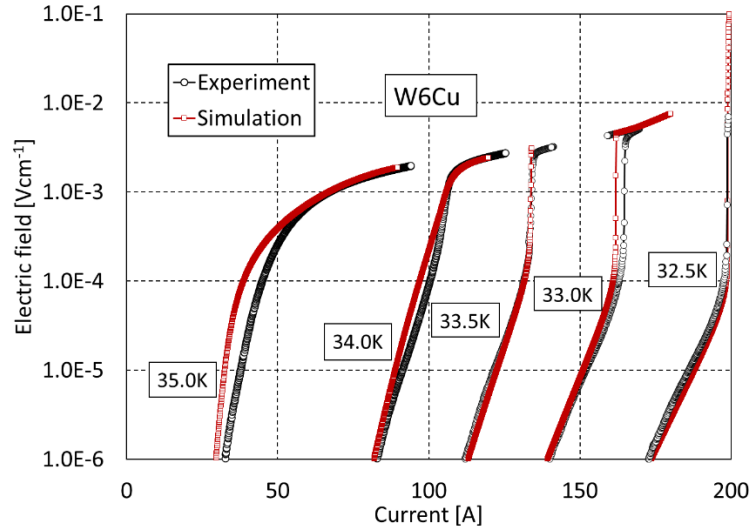


Figure 23 The comparison of E - I characteristics obtained on W6Cu by simulation and measurement under H_2O ice cooling condition.

Similar trend of shifting in I_c between the simulation and measurement is also evident for W6Nb. At lower critical currents, around 30 A, there exists an approximate 3 A disparity in I_c values. However, it diminishes with an increase in I_c , and at around 80 A, the difference in I_c values becomes negligible. As we explore the characteristics at higher values of E , a discernible difference in the shape of the curves is apparent at low currents. But, above the transport current of 100 A, the characteristics exhibit excellent similarity, both prior to quenching and after the transition to the normal state.

The model captures the experiment's temperature changes, even during thermal runaway, such as the one observed at $T = 32.5$ K and corresponding $I_c = 173$ A. This is related with an abrupt energy release during quench, resulting in apparent increase of sample's temperature. The Joule heating during this phase was so substantial that the temperature increase became uncontrollable.

It is important to note that, in our experimental setup, the temperature of the wire was sensed using a relatively large Cernox sensor. The larger dimensions of the sensor introduced potential inaccuracies, including a time delay due to its non-negligible mass and thermal capacity. Furthermore, it is likely that some errors were introduced by the heat transfer within the system. These factors should be taken into consideration when comparing and interpreting the temperature development between the simulation and the experimental data.

6 Conclusion

The enhancement of the engineering current density of MgB₂ wires is pivotal for their expected integration into future power systems, medical devices, and other advanced applications. Achieving a high current density can be accomplished by increasing the content of the MgB₂ phase within the wire. However, this requirement simultaneously influences other important properties, such as mechanical tolerance, AC losses and last but not least sufficient electro-thermal stability.

This work primarily focuses on investigating the electro-thermal stability of MgB₂ composite wires through transport measurements performed under various cooling conditions. This investigation was utilized in measuring systems designed for in-field measurements at variable temperatures. The design of cryogen-free system employed a cryocooler to reach temperatures as low as 10 K. The testing shows that a small amount of helium gas introduced into the system, resulting in significantly enhancement of overall cooling efficiency of whole cryogenic system represented by a cooling time reduction and increase in minimal reached temperature.

More in detail, the effect of different coolant on transport stability of multifilamentary MgB₂ wire was investigated by comparing E-I characteristics measured in GHe, SN₂ and H₂O ice. The quench power P_q , temperature of sample and I_q/I_c ratio were determined for various cooling conditions. The most stable behavior was observed for measurement in H₂O ice, where the quench occurs at one order of magnitude higher P_q than under all other cooling conditions. The I_q/I_c ratio reaches also the highest values at measurement in H₂O ice. Values comparable with other cooling conditions were in H₂O ice reached at almost double transport currents. Moreover, the H₂O ice allows stable operation of superconducting sample in normal state at currents below 200 A, which was not possible for other of used coolants. The stable, normal state operation of the wire was observed even its temperature exceeds ~50 K which was not even reachable in LHe.

Part of this work focuses on multi-pulse (MP) method suitable for alternative approach to determining Minimum Quench Energy (MQE). While the conventional method involves localized heating on the wire's surface, the MP method generates heat within the wire volume, providing a more reflective representation of operational instability formation. Hence, this method may be beneficial for future investigation of transport stability of superconducting wires, especially under varying cooling conditions.

An electrothermal model of multifilamentary composite wires was developed using commercial software COMSOL Multiphysics. The results of this simulation were compared with experimental results obtained through DC transport measurements performed in subcooled H₂O ice. The model accurately reproduced experimental results for Cu-stabilized multifilamentary wire. Slightly lower agreement was observed for Cu-free wire with considerably higher resistance, which was detailly explained in the corresponding section. The model offers valuable insights into temperature distribution and power dissipation rates during the normal operation as well the quench, which can be useful for the design and stability assessment of various devices in the future.

In summary, subcooled H₂O ice demonstrated excellent cooling properties, which was successfully proved in experimental parts of this work. Its high thermal conductivity and notable thermal capacity allowed for temperature homogenization along the wire and maintained stable operational temperatures during measurements. Additionally, H₂O ice provided reliable protection for the sample after quenching, resulting in only gradual and well controlled temperature increases during high power dissipation. During the testing process, there were not observed instances of degradation in the superconducting wires caused by mechanical compression in H₂O ice. Moreover, the H₂O ice is cost-effective, widely available and chemically stable, all these attributes predict to H₂O ice be a promising choice for future cryogen free systems or other superconducting devices and applications.

7 Bibliography

- [1] M. Tomsic, "Overview of MgB₂ Superconductor Applications," *International Journal of Applied Ceramic Technology*, vol. 4, no. 3, p. 250–259, 2007.
- [2] T. Nakamura, I. Muta, K. Okude, A. Fujio and T. Hoshino, "Solidification of nitrogen refrigerant and its effect on thermal stability of HTSC tape," *Physica C*, Vols. 372-376, pp. 1434-1437, 2002.
- [3] F. Gömöry, J. Šouc, M. Adámek, A. Ghabeli, M. Solovyov and M. Vojenciak, "Impact of critical current fluctuations on the performance of a coated conductor tape," *SUST*, vol. 32, no. 124001, p. 17pp, 2019.
- [4] R. C. Duckworth, J. W. Lue, D. F. Lee, R. Grabovickic and M. J. Gouge, "The Role of Nickel Substrates in the Quench Dynamics of Silver Coated YBCO Tapes," *IEEE TRANSACTIONS ON APPLIED SUPERCONDUCTIVITY*, vol. 13, no. 2, p. 3pp, 2003.
- [5] H. M. Kim, J. Jankowski, H. Lee, J. Bascuñán, S. Fleshler and Y. Iwasa, "Stability of Bare and Copper-Laminated YBCO Samples: Experimental & Simulation Results," *IEEE TRANSACTIONS ON APPLIED SUPERCONDUCTIVITY*, vol. 14, no. 2, p. 4pp, 2004.
- [6] R. Grabovickic, J. W. Lue, M. J. Gouge, J. A. Demko and R. C. Duckworth, "Measurements of Temperature Dependence of the Stability and Quench Propagation of a 20-cm-Long RABiTS Y-Ba-Cu-O Tape," *IEEE TRANSACTIONS ON APPLIED SUPERCONDUCTIVITY*, vol. 13pp, no. 2, p. 5pp, 2003.
- [7] J. E. Jankowski, Convective Heat Transfer Model for Determining Quench Recovery of High Temperature Superconducting YBCO in Liquid Nitrogen, Massachusetts: Massachusetts Institute of Technology, 2004.
- [8] M. Búran, L. Kopera, P. Kováč and I. Hušek, "Thermal stability of 6-filament MgB₂ wire cooled by liquid He and water ice," *Cryogenics*, vol. 133, no. 103694, 2023.
- [9] M. Búran, L. Kopera and P. Kováč, "Transport measurement of MgB₂ wire under the sub-cooled water ice compared to other cooling conditions," *SUST*, vol. 35, no. 105004, 2022.
- [10] C. LACROIX and F. SIROIS, "Concept of current flow diverter for accelerating normal zone propagation velocity in 2G HTS coated conductors.," *SUST*, vol. 27, no. 3, 2014.
- [11] C. LACROIX and F. SIROIS, "Impact of Current Flow Diverter on Innovative HTS Tape Architectures for DC Fault Current Limitation at Electric Field up to 150 V/m," *IEEE*, vol. 29, no. 5, 2019.
- [12] C. Koyunoğlu, Temperatures, Thermal Properties on Metals at Cryogenic, Heat and Mass Transfer - Advances in Science and Technology Applications, Tokio: IntechOpen, 2018.
- [13] L. Robert, A. Powell and W. Blanpied, Thermal Oanductivity of Metals and Alloys at low temperature - A Review of the Literature, Washington: UNITED STATES DEPARTMENT OF COMMERCE, 1954.

Publications

List of scientific papers (2021-2023):

Kováč, P., Kováč, J., Perez, N., Scheiter, J., **Búran, M.**, Kopera, L., ... & Berek, D. (2021). Low-purity Cu and Al sheathed multi-core MgB₂ wires made by IMD process. *Superconductor Science and Technology*, 34(7), 075010.

Mošať, M., Šouc, J., Vojenčiak, M., Solovyov, **M.**, **Búran, M.**, & Gömöry, F. (2021). Influence of current change rate during DC current limitation on the coated conductor degradation. *IEEE Transactions on Applied Superconductivity*, 31(5), 1-5.

Búran, M., Kováč, P., Kopera, L., & Melišek, T. (2021). IV characteristics of MgB₂ conductors with different metallic sheaths. *Cryogenics*, 120, 103370.

Kováč, P., Melišek, T., Kováč, J., **Búran, M.**, Hušek, I., Rindfleisch, M., & Tomsic, M. (2022). DC characterization of advanced fine-filamentary MgB₂ superconducting wires. *Superconductor Science and Technology*, 35(5), 055004.

Kováč, P., Kopera, L., Melišek, T., **Búran, M.**, Hušek, I., Berek, D., & Kováč, J. (2022). Water ice-cooled MgB₂ coil made by wind and react process. *Superconductor Science and Technology*, 35(5), 055001.

Kováč, P., **Búran, M.**, & Kopera, L. (2022). Behaviour of Al₂O₃-oxide insulated and non-insulated superconducting MgB₂ coils cooled by water ice. *Superconductor Science and Technology*, 35(9), 095007.

Búran, M., Kopera, L., & Kováč, P. (2022). Transport measurement of MgB₂ wire under the sub-cooled water ice compared to other cooling conditions. *Superconductor Science and Technology*, 35(10), 105004.

Kováč, P., Kopera, L., Berek, D., Hain, M., Melišek, T., Hušek, I., **Búran, M.** (2022). High-current-density Rutherford MgB₂ cable sheathed by CuNi30 alloy. *Superconductor Science and Technology*, 35(11), 115003.

Kováč, P., Berek, D., Melišek, T., Kováč, J., Hušek, I., **Búran, M.**, Choi, J. H. (2023). Influence of filament number and size on the basic properties of in situ made MgB₂ wires. *Superconductor Science and Technology*, 36(4), 045014.

Búran, M., Kováč, P., Kopera, L., & Hušek, I. (2023). Thermal stability of 6-filament MgB₂ wire cooled by liquid He and water ice. *Cryogenics*, 103694.

Srivastava, N., Mehrotra, S., **Búran, M.**, Hušek, I., Sharma, D., Kováč, P., & Santra, S. (2023). Interfacial reactions and critical current density of Cu-sheathed Cu-doped MgB₂ wire with Ti diffusion barrier. *Journal of Alloys and Compounds*, 966, 171657.

Srivastava, N., Mehrotra, S., Sharma, D., **Búran, M.**, Hušek, I., Goswami, A., Santra, S. (2023). Effect of wire diameter on structure and electrical properties of (Al+ Al₂O₃)-sheathed MgB₂ with Nb barrier. *Ceramics International*, 49(22), 34627-34637.

Búran, M., Kopera, L., Melišek, T., & Kováč, P. (2023). E-I characteristics and critical currents of small Bi-2223/Ag coil thermally stabilized by solid and liquid nitrogen compared to water ice. *Superconductor Science and Technology*, 36(10), 105013.

List of conference proceedings (2022-2023):

Búran, M., Kopera, L., & Kováč, P. (2022) *Behaviour of MgB₂ wire inside the liquid Helium and sub-cooled water ice*, MEMS 2022, Poster section, Karlsruhe, Germany

Búran, M., Kopera, L., & Kováč, P. (2023). *Stability of MgB₂ wires under different cooling conditions*. EUCAS 2023, Poster section, Bologna, Italy

List of scientific papers (2019-2020):

Búran, M., Vojenčiak, M., Mošať, M., Ghabeli, A., Solovyov, M., Pekarčíková, M., ... & Gömöry, F. (2019). Impact of a REBCO coated conductor stabilization layer on the fault current limiting functionality. *Superconductor Science and Technology*, 32(9), 095008.

Pekarčíková, M., Mišík, J., Drienovský, M., Krajčovič, J., Vojenčiak, **M.**, **Búran, M.**, ... & Gömöry, F. (2020). Composite heat sink material for superconducting tape in fault current limiter applications. *Materials*, 13(8), 1832.

Monograph:

JANÍČEK, František, **Marek BÚRAN**, Anton CERMAN, Tomáš HANUS, Juraj KUBICA a Miriam SZABOVÁ. *Obnoviteľné zdroje na Slovensku a ich vplyv na elektrizačnú sústavu*. Bratislava: Slovenská technická univerzita v Bratislave, 2019. Edícia vedeckých monografií. ISBN 978-80-227-4966-4.